Supplementary Figures

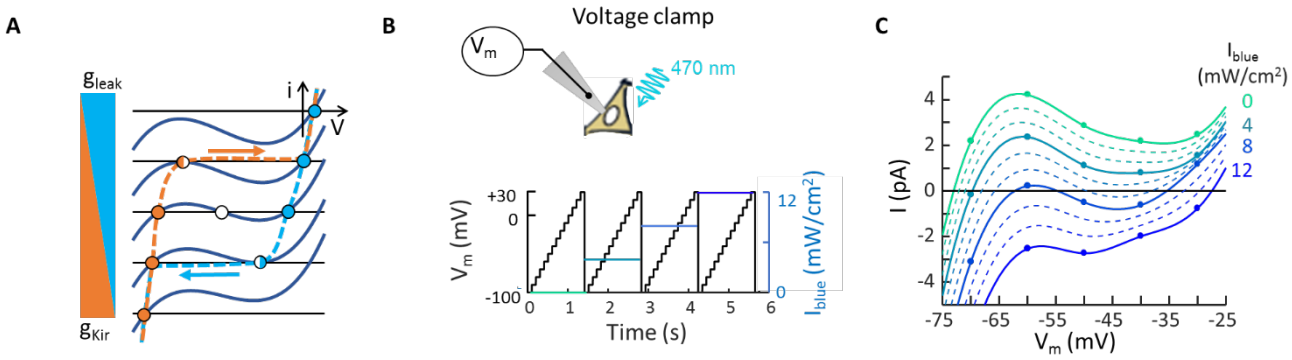

Supplementary Figure 1. Electrophysiological characterization of bi-HEK cells. A) Cartoon showing origin of bistability in cells expressing a K_{ir} channel and a leak conductance. Changes in the ratio of leak to K_{ir} conductance drive the *I-V* curve through two saddle-node bifurcations. B) Protocol for measuring the *I-V* curve under different levels of optogenetic drive. Measurements were performed in voltage clamp mode. C) Patch clamp measurements of the *I-V* curve of a small island of bi-HEKs under varying blue light illumination. Points represent measurements. Dotted lines are interpolations.

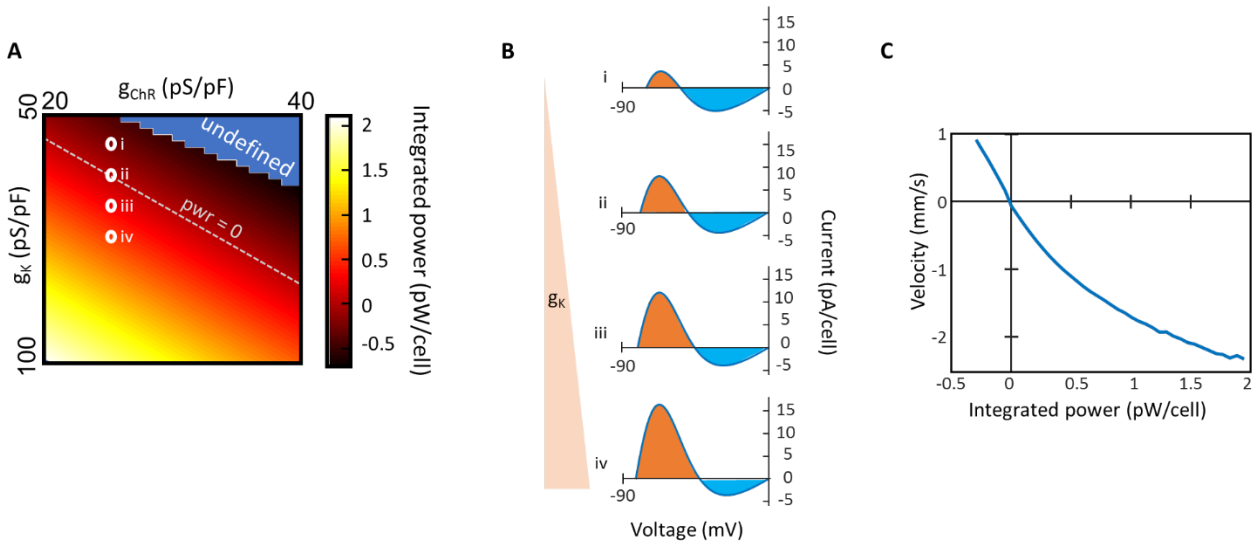

Supplementary Figure 2. Balance of ionic currents determines velocity of domain wall motion in homogeneous tissues. The balance of currents is set by the integral of the *I-V* curve between the two stable fixed points, or equivalently the relative areas of the orange and blue shaded regions in panel (B). The area under the curve ($\int IdV$) has units of power. A) Area under the *I-V* curve as a function of the $K_{ir}2.1$ and channelrhodopsin conductance levels. The white dotted line corresponds to a stationary domain boundary. In the blue region there is only one stable fixed point (near V = 0), so the area under the curve is undefined. B) Example *I-V* curves from the corresponding circled regions in (A). C) Domain wall velocity as a function of the area under the *I-V* curve. Positive velocities indicate growth of the depolarized domain.

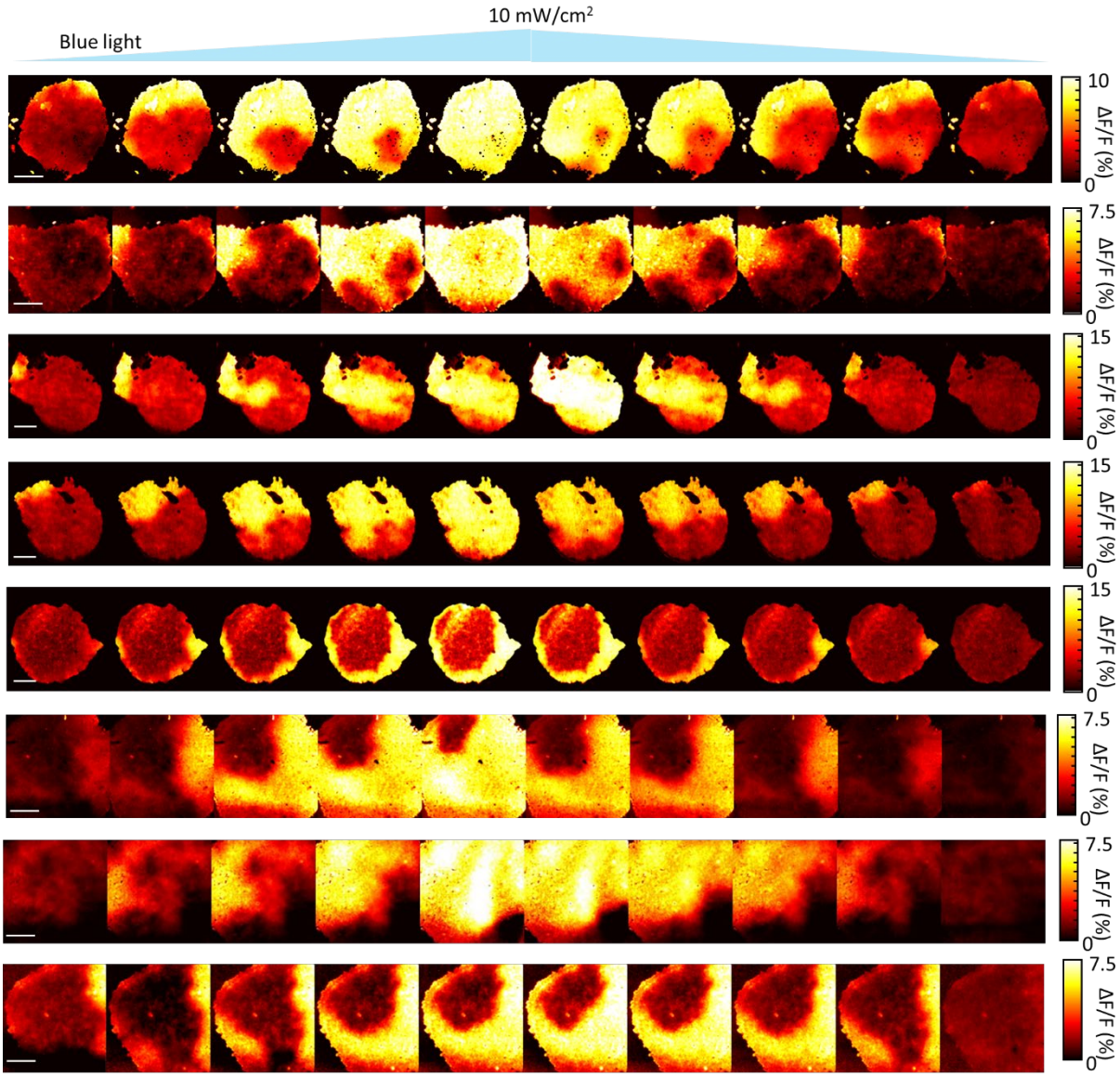

Supplementary Figure 3. Bioelectrical domain wall formation in eight distinct islands. Each island showed a unique pattern of domain wall nucleation and growth. In some islands the optogenetic drive was not sufficiently powerful to depolarize the entire island. Scale bars 1 mm.

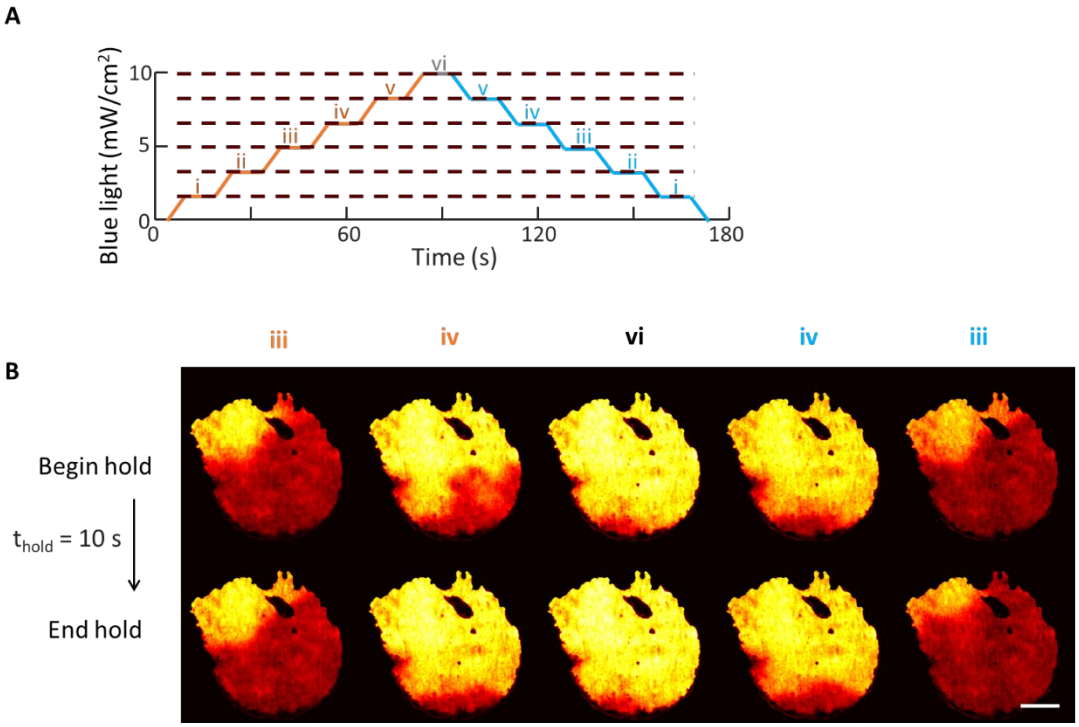

Supplementary Figure 4. Stability of bioelectrical domain walls. A) Optogenetic stimulation comprised alternating ramps and 10 s pauses. B) During each pause the domain wall profile remained stable. Slight drifts in domain wall position occurred at the beginning of some hold periods due to slow switching of domains nearly balanced between depolarized and polarized states. Scale bar 1 mm.

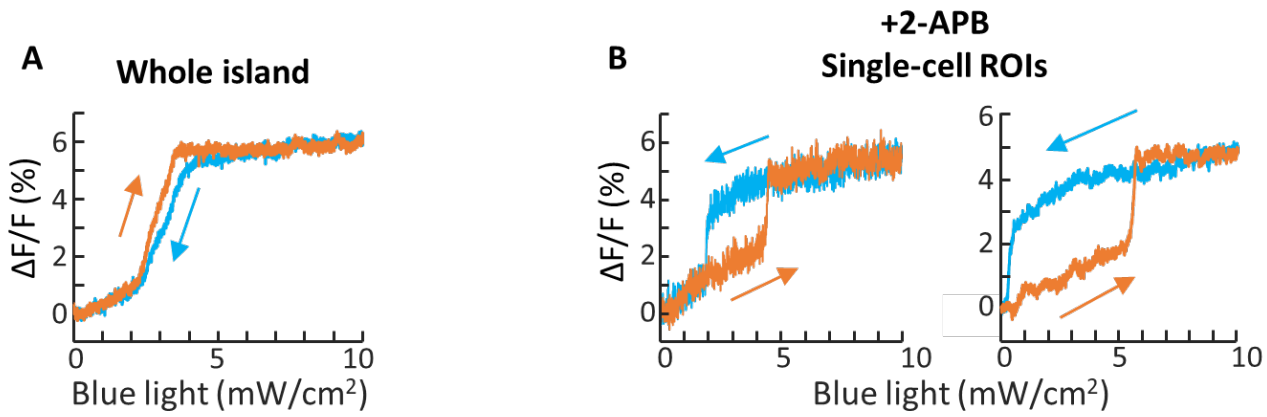

Supplementary Figure 5. Gap junction blockers convert 2-D behavior in an island to an ensemble of independent 0-D systems. A) Fluorescence as a function of optogenetic stimulation strength in a confluent island of bi-HEK cells. B) Two single-cell regions from the island after addition of gap junction blocker 2-APB (50 μM). Each cell developed a hysteresis loop with transitions set by the local $K_{ir}2.1$ and CheRiff expression levels.

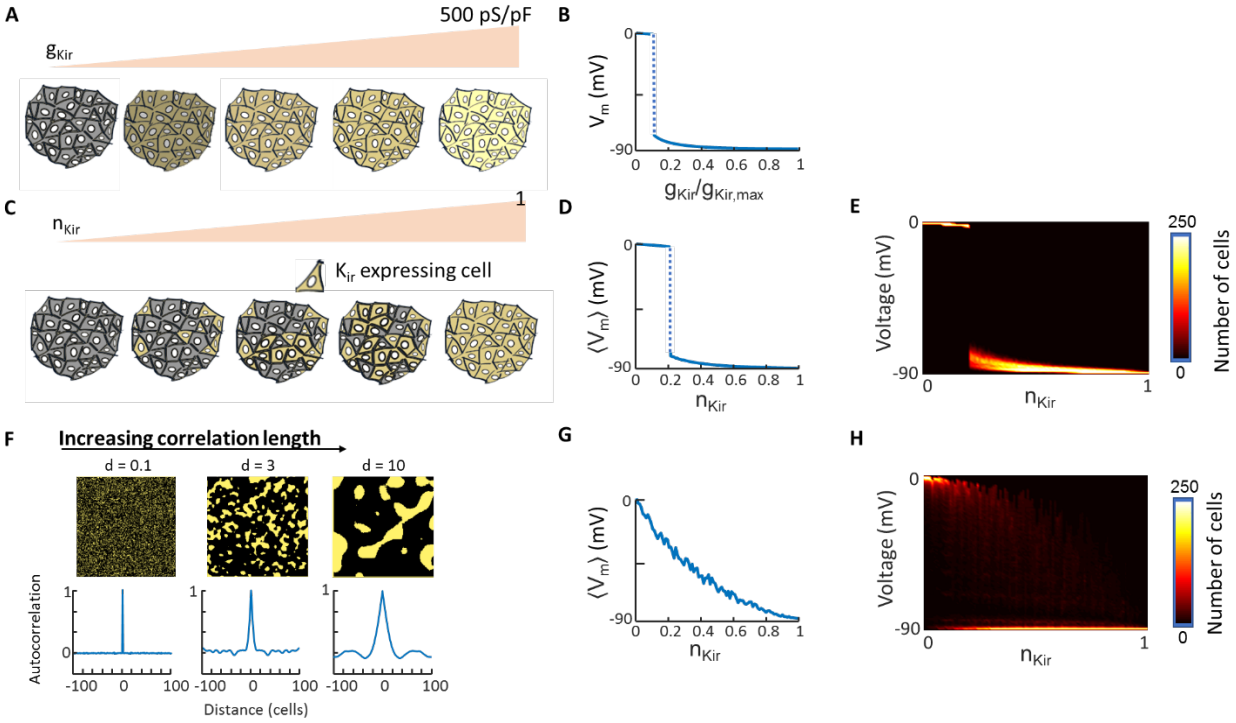

Supplementary Figure 6. Effect of noisy gene expression on domain wall properties. A) Cartoon showing a homogeneous tissue with constant leak conductance and gradually increasing $K_{ir}2.1$ conductance. B) Membrane voltage (V_m) as a function of g_{Kir}. Abrupt polarizing transition arises when g_{Kir} is sufficient to drive polarized domain wall growth. C) Cartoon showing a heterogeneous tissue where the fraction of cells that express $K_{ir}2.1$ gradually increases. In this cartoon the probability of expression is independent in each cell. D) As in the homogeneous tissue, at a critical expression density the tissue-average voltage polarizes in a step-wise manner due to domain wall migration. E) Probability distribution of single-cell voltage values as a function of n_{Kir}. In the heterogeneous tissue, the voltage can vary between cells, though when the size of each cell is much smaller than the domain wall width, $\lambda \sim \sqrt{\frac{G_{cxn}}{g_K}}$, then the distribution of single-cell voltages is narrowly centered around the mean. F) Introduction of spatially correlated gene expression in models of bi-HEK cells. Top: example images of $K_{ir}2.1$ expression with different degrees of spatial correlation. Bottom: radially averaged autocorrelation functions of the simulated tissues shown above. G) Tissue-average membrane potential as a function of n_{Kir} in the case of correlated disorder (d = 10 cells). The step-wise transition to polarization is replaced by a patchwork of polarized and depolarized domains. Changes in n_{Kir} change the relative populations of these two domains. H) Probability distribution of single-cell voltage values as a function of n_{Kir} in the tissue simulated in (G).

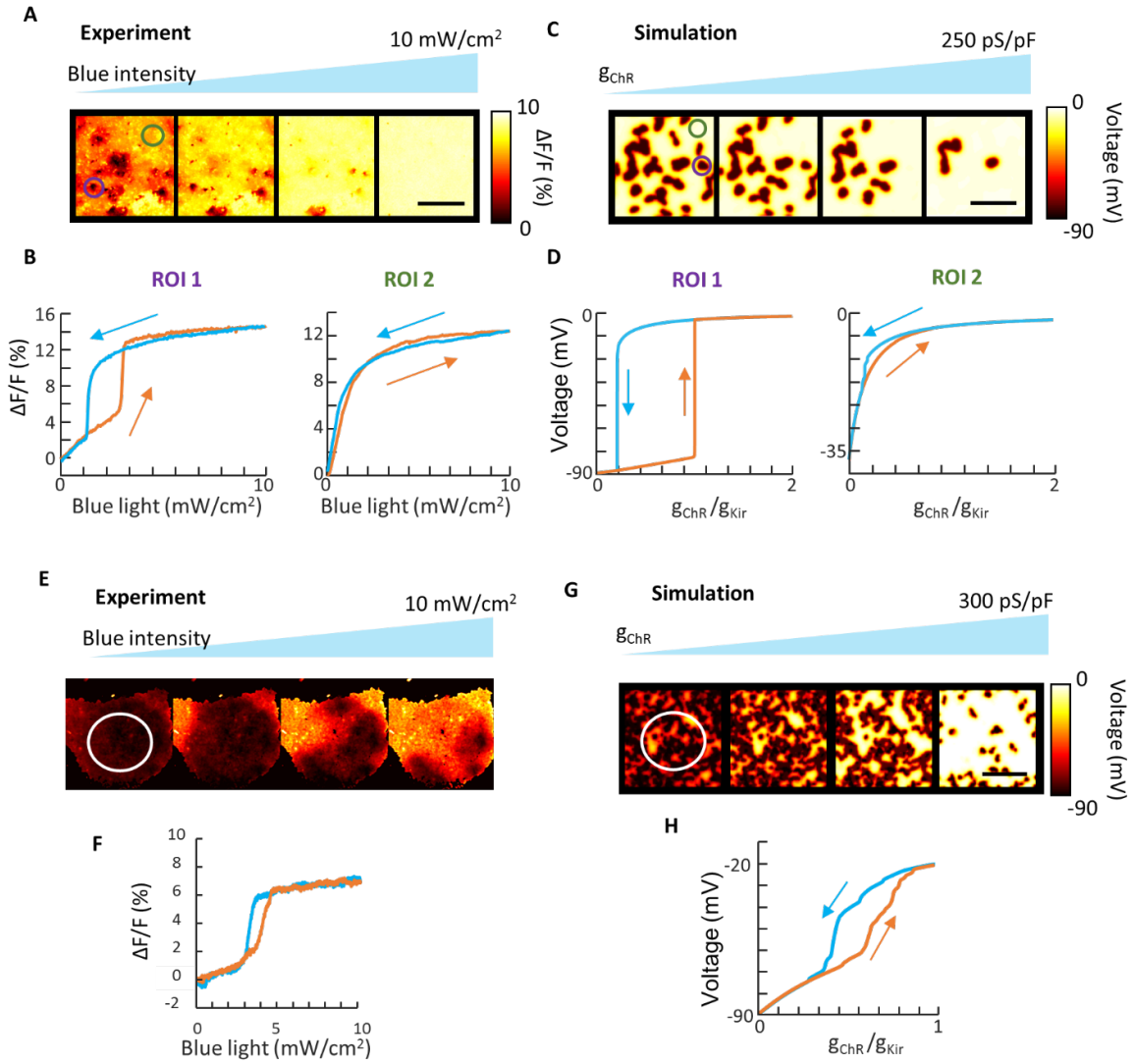

Supplementary Figure 7. Spatially correlated variability in K_{ir}2.1 expression drives breakup of tissues into discrete domains. A monoclonal cell line expressing CheRiff only was transfected with plasmid for K_{ir}2.1 and then allowed to grow for 3 days to reach confluence, leading to clusters of correlated expression ~3 cells wide. Calibration transfections with a fluorescent marker showed that only ~30% of the cells expressed. A) Images of fluorescence increase ($\Delta F/F$) in a heterogeneous culture under ramped optogenetic stimulation. Scale bar 1 mm. B) Plots of fluorescence from the two indicated regions of interest (ROIs) in (A). Some ROIs showed hysteresis while others showed smooth and reversible depolarization. C) Frames from a simulation with noisy K_{ir}2.1 expression and ramped optogenetic drive. Scale bar 0.5 mm. D) Regions of the simulation showed ROIs with hysteresis and others without. E) Island of bi-HEK cells driven with a triangle wave of blue light showing depolarization via domain wall migration. F) Fluorescence averaged over the circled region in (E), showing partial hysteresis and Barkhausen-like noise in a disordered sample. G) Simulation of depolarization of a noisy tissue under ramped optogenetic stimulation. H) Mean voltage in the circled region in (G) showing partial hysteresis and Barkhausen-like noise in a disordered sample.

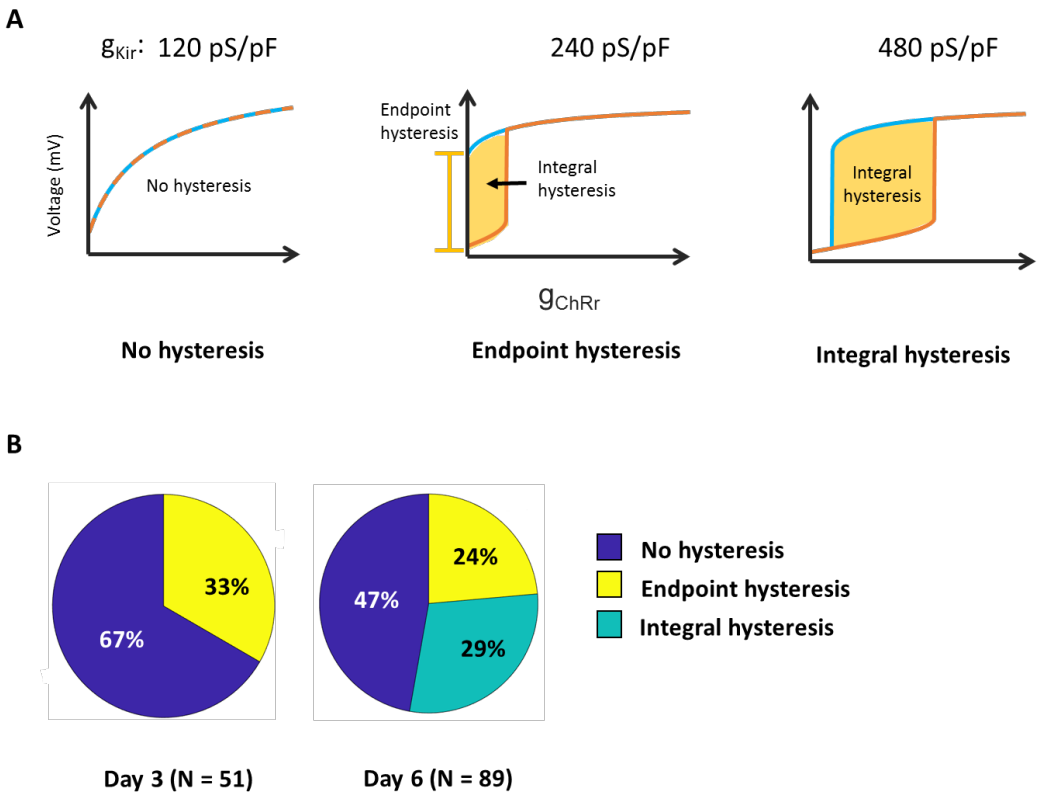

Supplementary Figure 8. Electrophysiological phenotypes in immature isolated myocytes. A) Definition of electrophysiological classes showing "No hysteresis", "Endpoint hysteresis" and "Integral hysteresis". The plots show numerical simulations of the K_{ir} + leak + ChR model with increasing levels of K_{ir} and all other parameters held constant. B) Distribution of phenotypes by day of measurement. Smooth depolarizations without hysteresis were observed on day 3 in 34 of 51 cells and on day 6 in 42 of 89 cells, a significant decrease (P = 0.026). Endpoint hysteresis was observed on day 3 in 17 of 51 cells and on day 6 in 26 of 89, not a significant difference (P = 0.61). Integral hysteresis was observed on day 3 in 0 of 51 cells and on day 6 in 21 of 89 cells (P < 0.001). Statistical errors in the population fractions were estimated as the standard deviation from a binomial distribution; i.e., $\sigma = \sqrt{Np(1-p)}$. The significance of population level phenotypes was assessed via paired two-sample t-tests using standard MATLAB functions (ttest2).

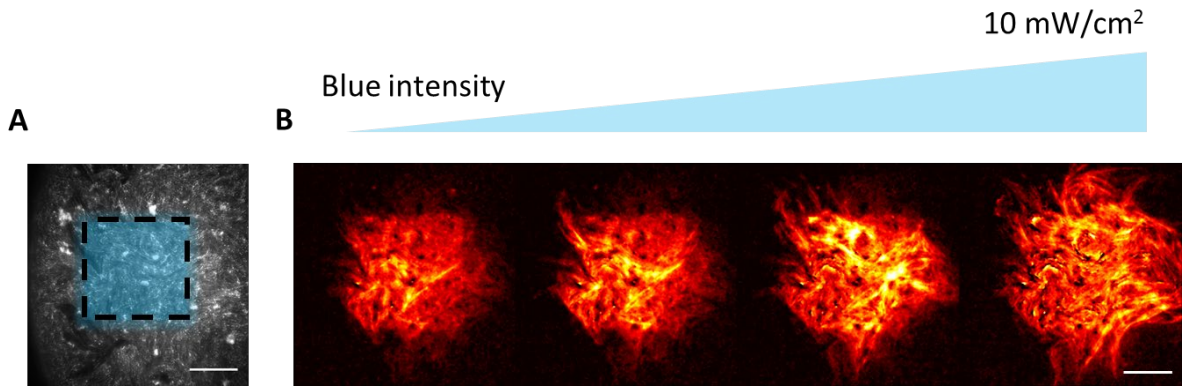

Supplementary Figure 9. Gap junction coupling in confluent cultures of immature myocytes. A) image of the myocyte culture showing region of cells stimulated with blue light. B) Fluorescence of BeRST1 indicating electrical depolarization as a function of optogenetic stimulus strength. Propagation of the depolarization to cells outside the stimulated region establishes the presence of gap junction-mediated electrical coupling in the culture. Scale bars 1 mm.

Supplementary Movie Captions

Supplementary Movie S1: Simulation of nucleation and growth of bioelectrical domains in homogeneous tissue

Supplementary Movie S2: Nucleation and growth of bioelectrical domains in a confluent culture of bi-HEK cells, example 1

Supplementary Movie S3: Nucleation and growth of bioelectrical domains in a confluent culture of bi-HEK cells, example 2

Supplementary Movie S4: Switching of discrete bistable bioelectrical domains in disordered culture of bi-HEK cells

Supplementary Movie S5: Simulation of switching of discrete bistable bioelectrical domains in disordered tissue

Supplementary Movie S6: Depolarization via domain wall propagation in a confluent culture of human iPSC-derived myocytes